

Journal of Biomedical Optics

BiomedicalOptics.SPIEDigitalLibrary.org

Computationally efficient error estimate for evaluation of regularization in photoacoustic tomography

Manish Bhatt
Atithi Acharya
Phaneendra K. Yalavarthy

SPIE.

Manish Bhatt, Atithi Acharya, Phaneendra K. Yalavarthy, "Computationally efficient error estimate for evaluation of regularization in photoacoustic tomography," *J. Biomed. Opt.* **21**(10), 106002 (2016), doi: 10.1117/1.JBO.21.10.106002.

Computationally efficient error estimate for evaluation of regularization in photoacoustic tomography

Manish Bhatt, Atithi Acharya, and Phaneendra K. Yalavarthy*

Indian Institute of Science, Medical Imaging Group, Department of Computational and Data Sciences, C V Raman Avenue, Bengaluru 560012, India

Abstract. The model-based image reconstruction techniques for photoacoustic (PA) tomography require an explicit regularization. An error estimate (η_2) minimization-based approach was proposed and developed for the determination of a regularization parameter for PA imaging. The regularization was used within Lanczos bidiagonalization framework, which provides the advantage of dimensionality reduction for a large system of equations. It was shown that the proposed method is computationally faster than the state-of-the-art techniques and provides similar performance in terms of quantitative accuracy in reconstructed images. It was also shown that the error estimate (η_2) can also be utilized in determining a suitable regularization parameter for other popular techniques such as Tikhonov, exponential, and nonsmooth (ℓ_1 and total variation norm based) regularization methods. © 2016 Society of Photo-Optical Instrumentation Engineers (SPIE) [DOI: [10.1117/1.JBO.21.10.106002](https://doi.org/10.1117/1.JBO.21.10.106002)]

Keywords: photoacoustic tomography; error estimate; regularization; image reconstruction.

Paper 160419RR received Jun. 17, 2016; accepted for publication Sep. 14, 2016; published online Oct. 20, 2016.

1 Introduction

Photoacoustic tomography (PAT) is a rapidly growing noninvasive, *in vivo* hybrid biomedical imaging technique combining both optics and acoustics. It has applications in breast cancer imaging, brain imaging, temperature monitoring, sentinel lymph node imaging, and so on.^{1–6} It holds a great potential for anatomical, functional, and molecular imaging in preclinical and clinical medicine.^{6–9} In PAT, to-be-imaged biological tissue is illuminated with a nanosecond laser pulse, which generates internal acoustic wavefields through the thermoacoustic effect.⁶ The initial amplitude of induced acoustic wavefield (pressure rise) is proportional to the absorbed optical energy density in the tissue. These acoustic wavefields propagate out of the tissue and are measured by the use of an array of ultrasonic transducers. From the measured acoustic data, an image reconstruction algorithm, analytical, or model-based in nature,^{10–14} is employed to obtain an estimate of the image that depicts the initial pressure rise or the spatially variant optical energy density distribution within the imaged tissue.

Many analytical image reconstruction algorithms have been proposed in the literature.¹⁵ These algorithms, in the form of filtered back projection, are based on spherical Radon transform. They require a large amount of data to accurately estimate the initial pressure distribution. Large data acquisition needs expensive ultrasonic transducer arrays along with increased data collection time when a mechanical scanning is employed. Moreover, the analytical algorithms do not provide much required quantitative accuracy in limited data cases.¹⁶

Model-based image reconstruction algorithms^{15,16} can improve image quality in these limited data cases and have a larger utility for practical scenarios. Thus, development and investigation of model-based algorithms for PAT image reconstruction is an important research topic of current interest. In limited-data case, the regularized least-squares QR (LSQR)

based image reconstruction scheme was earlier deployed by our group¹⁷ and proven to be highly efficient and quantitatively more accurate in providing regularized solution.^{17,18} Traditional regularization schemes, such as Tikhonov regularization, become relatively expensive in terms of computation with a requirement of having an explicit appropriate regularization parameter.

Photoacoustic (PA) image reconstruction problem deals with estimation of initial condition of an observed effect. This is a discrete ill-posed problem, where the system matrix is ill conditioned in nature. The computation of numerical solution is challenging due to the possibility of severe error propagation (caused by measurement inaccuracies, transmission errors of the data, and discretization errors). The regularized solutions, such as Tikhonov regularization, reduce the sensitivity of the computed solution to errors in the data. These regularization methods require a suitable value of regularization parameter to be chosen. In this study, we investigate a class of error estimates (η_2) for the approximate solution and propose to apply this error estimate to compute a suitable value of the regularization parameter. This study focuses on the widely popular Tikhonov regularization framework, which uses Lanczos bidiagonalization to provide dimensionality reduction to the system matrix in case of limited-view datasets.^{17,18} The applications of the proposed error estimates to various direct and iterative regularization methods were also discussed, and the effectiveness of this analysis is proven by extensive numerical experimentation. It is proven that the class of error estimate that is proposed here is very effective and computationally efficient for evaluation of regularization in PA imaging.

2 Forward Problem in Photoacoustic Tomography: System Matrix Approach

A system matrix-based approach was utilized,¹⁸ where the PA system is represented by a Toeplitz matrix of a time-varying

*Address all correspondence to: Phaneendra K. Yalavarthy, E-mail: phani@cds.iisc.ac.in

causal system. This approach was extensively discussed in Refs. 17 and 18, herein it is only briefly reviewed.

The image representing the imaging domain, having a dimension of $n \times n$, is vectorized by stacking all columns in lexicographic manner, converting it into a $n^2 \times 1$ size vector. This vector was represented as x , the unknown to be estimated in the PA inverse problem. The time varying PA data collected at the ultrasonic transducers was also stacked into a $m \times 1$ dimensional vector, represented as the measurement vector b . The PA system matrix (\mathbf{A}) has a dimension of $m \times n^2$, each column representing impulse response (IR) of a corresponding pixel in the image, as explained in Refs. 17 and 18. The k-Wave toolbox,¹⁹ which simulates the acoustic wave propagation in two dimension, was utilized to construct the PA system matrix. This simulation is computationally expensive to perform for all pixels. To reduce the computational time for building the system matrix, IR is recorded for only one pixel (corner pixel), and IRs for the rest of the pixels were determined using the shifting and attenuation properties of PA signal. The IRs for all pixels are computed and filled in column-by-column in the system matrix form.

It was assumed that the medium has homogeneous ultrasound properties. The sound of speed was modeled to be 1500 m/s (approximate value for typical soft tissues). The ultrasound detectors were considered to be point detectors with a frequency response of 2.25 MHz as center frequency and 70% bandwidth. These detectors were placed equidistantly around a 22-mm radius circle. A perfectly matched layer was used to satisfy the boundary condition. The simulation geometry had a k-Wave computational grid of size 501×501 pixel size, each pixel measuring 0.1 mm (50 mm \times 50 mm). The imaging domain had 201×201 pixels ($n^2 = 40,401$). The time step for data collection was 50 ns, with a total of 500 steps. For a total of 60 detectors' geometry, $m = 60 \times 500$. Thus the size of the system matrix ($m \times n^2$) becomes $30,000 \times 40,401$.

To summarize, the forward model of PA imaging can be expressed as

$$\mathbf{A}x = b, \quad (1)$$

where \mathbf{A} is the system matrix (collection of IRs of each pixel), x is initial pressure value (unknown) for each pixel in the imaging domain, and b is the vector containing the recorded measurement data from ultrasound transducers.

3 Error Estimate for a Regularized Solution

The error (e) in the measurement vector (b), also referred as noise, can be caused by measurement inaccuracies and discretization errors. Let $\hat{b} \in \mathbb{R}^m$ (unavailable) be the noise-free vector associated with b :

$$b = \hat{b} + e, \quad (2)$$

and let $\hat{x} \in \mathbb{R}^{n^2}$ be the minimal-norm least squares solution of the following problem,

$$\arg \min_{x \in \mathbb{R}^{n^2}} \|\mathbf{A}x - b\|_2^2. \quad (3)$$

Here, $\|\cdot\|_2$ represents ℓ_2 norm. The aim of the PA inverse problem is to estimate the initial pressure distribution, x , from the above equation.^{17,18} In order to compute a useful approximation, the minimization problem is replaced by a nearby problem,

which is less sensitive to noise in b , also known as Tikhonov regularization. The cost function minimization for this problem becomes

$$x_\lambda = \arg \min_{x \in \mathbb{R}^{n^2}} \|\mathbf{A}x - b\|_2^2 + \lambda \|\mathbf{R}x\|_2^2, \quad (4)$$

where $\lambda > 0$ is a regularization parameter and \mathbf{R} is a regularization operator. For the conventional Tikhonov regularization $\mathbf{R} = \mathbf{I}$; other possible choices of \mathbf{R} are discussed in Ref. 20. The minimization of cost function in Eq. (4) leads to the solution

$$x_\lambda = (\mathbf{A}^T \mathbf{A} + \lambda \mathbf{I})^{-1} \mathbf{A}^T b, \quad (5)$$

for any $\lambda > 0$. The regularization parameter (λ) determines the sensitivity of the solution x_λ to the noise/error e in b , and how close x_λ would be to, \hat{x} , the desired solution of Eq. (3). Thus, determining a suitable choice of λ is a very important part of finding solution. This work addresses this problem and proposes a method based on error estimates to find the regularization parameter.

The initial pressure rise (x) in the imaging domain is unknown in experiments. The associated residual vector is defined to be $r := \hat{b} - \mathbf{A}x$. Brezinski et al.²¹ derived the family of error estimates for the norm of the difference, i.e., $d = x - \hat{x}$, given as²²

$$\|d\|_2^2 \approx \eta_\nu^2 := d_o^{\nu-1} d_1^{5-2\nu} d_2^{\nu-3}, \quad \nu \in \mathbb{R}, \quad (6)$$

where

$$d_o := \|r\|_2^2, \quad d_1 := \|\mathbf{A}^T r\|_2^2, \quad d_2 := \|\mathbf{A} \mathbf{A}^T r\|_2^2. \quad (7)$$

Proceeding from Eq. (6), the error estimate for $\nu = 2$ can be defined as

$$\eta_2 = \frac{\|r\|_2 \|\mathbf{A}^T r\|_2}{\|\mathbf{A} \mathbf{A}^T r\|_2}. \quad (8)$$

Since the noise-free measurement vector (\hat{b}), and the true solution (x) is not available, the residual vector (r) in Eq. (7) is written as

$$r = r_\lambda := b - \mathbf{A}x_\lambda. \quad (9)$$

The regularization parameter (λ) is determined by the minimization of the expression in Eq. (8):

$$\lambda = \arg \min_{\lambda \in \mathbb{R}_{>0}} \eta_2(\lambda) = \arg \min_{\lambda \in \mathbb{R}_{>0}} \frac{\|r_\lambda\|_2 \|\mathbf{A}^T r_\lambda\|_2}{\|\mathbf{A} \mathbf{A}^T r_\lambda\|_2}. \quad (10)$$

Note that in this work, only an approximation to $\eta_2(\lambda)$ was utilized (achieved through step 2 of Algorithm 1), thus removing the requirement of computing r_λ to find λ . However, Shaw et al.¹⁷ utilized the $\|r_\lambda\|_2^2$, which requires estimation of x_λ , which involves matrix-matrix operations. If the singular value decomposition (SVD) of the system matrix (\mathbf{A}) is available, the computation of residual r [Eq. (9)] and the estimates [Eq. (6)] is inexpensive. However, it may not be the case and as \mathbf{A} is large, these computations become expensive in the Tikhonov regularization framework. The cost efficiency of the system can be accomplished by reducing the matrix \mathbf{A} to a small lower bidiagonal matrix by applying few steps of Lanczos

Algorithm 1 Algorithm for evaluation of regularization parameter and number of Lanczos bidiagonalization steps.

Input: $\mathbf{A}; b; [\lambda_{\min}, \lambda_{\max}]; k_{\max} = \text{max number of Lanczos bidiagonalization steps}$

Output: Required number of Lanczos iterations: k ; regularization parameter: λ

1 Make a grid of q log-equispaced values of λ in the interval $[\lambda_{\min}, \lambda_{\max}]$. Define $S_1 := \{\lambda_1, \lambda_2, \dots, \lambda_q\}$ and $S_2 := \emptyset$.

2 For each λ_j in S_1 , compute the lower bound $\eta_2^l(\lambda_j)$, the upper bounds $\eta_2^u(\lambda_j)$, and their average $\bar{\eta}_2(\lambda_j)$. (Refer Theorem 3.1 of Ref. 22).

3 Find the smallest index p , such that

$$|\eta_2^u(\lambda_j) - \eta_2^l(\lambda_j)| < \beta \cdot \bar{\eta}_2(\lambda_j); \quad j = p, p+1, \dots, \#S_1, \quad (11)$$

where β is user specified tolerance (typically, 10^{-4}) and $\#S_1$ is the cardinality of the set S_1 .

4 if For above p 'th index, Eq. (11) = true then

5 Move $\{\lambda_p, \lambda_{p+1}, \dots, \lambda_{\#N}\}$ from S_1 to S_2

6 End

7 Increase $k := k + 1$, i.e., perform another Lanczos bidiagonalization step and repeat the algorithm steps 1 to 5 until

$$\bar{\eta}_2(\lambda_p) > \bar{\eta}_2(\lambda_{p+1})$$

for some pair $\{\lambda_p, \lambda_{p+1}\} \subset S_2$, this gives local minima λ^* of the function $\bar{\eta}_2(\lambda)$ and k is the corresponding number of Lanczos steps.

8 Add points around λ^* , by bisection in log-scale, to refine the set S_2 .

9 Repeat step 3. Update value of λ^* .

10 if $\lambda^* - \lambda_{\text{adjacent}} < \text{tolerance}$ (10^{-4}) then

11 Required $\lambda = \lambda^*$;

12 Else

13 Repeat steps 8 to 11;

14 End

bidiagonalization.^{17,18} This framework for PA image reconstruction with the application of proposed regularization method is described in next section.

3.1 Regularized LSQR Method

The equations of Lanczos bidiagonalization can be written as²³

$$\mathbf{G}_{k+1}(\beta_0 e_1) = b, \quad (12)$$

$$\mathbf{A}\mathbf{H}_k = \mathbf{G}_{k+1}\mathbf{B}_k, \quad (13)$$

$$\mathbf{A}^T\mathbf{G}_{k+1} = \mathbf{H}_k\mathbf{B}_k^T + \alpha_{k+1}h_{k+1}e_{k+1}^T, \quad (14)$$

where \mathbf{G}_k and \mathbf{H}_k represent the left and right orthogonal Lanczos matrices, β_0 represents the l_2 norm of b , e_1 as a unit vector of

dimension $k \times 1$, and \mathbf{B}_k represents the lower bidiagonal matrix having α_k in the main diagonal. The cost function can now be written as^{18,24}

$$\Omega = \|\beta_0 e_1 - \mathbf{B}_k x^{(k)}\|_2^2 + \lambda \|x^{(k)}\|_2^2,$$

where $x^{(k)}$ is the dimensionality reduced version of x , such that $k < n^2$. The updated equation for the solution estimate is given as

$$x_{\text{est}}^{(k)} = (\mathbf{B}_k^T \mathbf{B}_k + \lambda I)^{-1} \beta_0 \mathbf{B}_k^T e_1. \quad (15)$$

Once $x_{\text{est}}^{(k)}$ is estimated, then the initial pressure distribution can be obtained using the relation $p_o = x = \mathbf{H}_k x_{\text{est}}^{(k)}$.

Determining the required number of Lanczos bidiagonalization steps (k) and the regularization parameter (λ) using the error estimate (η_2) is given in Algorithm 1. We start the process with a grid of q log-equispaced values of λ in the interval $[\lambda_{\min}, \lambda_{\max}]$:

$$0 < \lambda_1 < \lambda_2 < \dots < \lambda_q. \quad (16)$$

These grid points are divided into two sets, S_1 and S_2 , as discussed in the Algorithm 1. The algorithm has two phases, the first phase computes a nearby estimate of the suitable regularization parameter λ^* . The initialization starts with $S_1 := \{\lambda_1, \lambda_2, \dots, \lambda_q\}$ and $S_2 := \emptyset$. The upper and lower bounds of the error estimate, $\eta_2(\lambda)$, can be computed with the help of Gauss–Radau quadrature rules, as described in Theorem 3.1 of Ref. 22. A smallest λ_p within the set S_1 was searched such that the absolute difference of upper and lower bound is smaller than a set threshold [See Eq. (11)]. Once this λ_p is found, all parameters in set S_1 after p 'th index will be moved to set S_2 . This indicates that $\bar{\eta}_2(\lambda_j)$ was considered as an approximation of $\eta_2(\lambda_j)$ for $j = p, p+1, \dots, \#S_1$.²² Now the number of Lanczos bidiagonalization steps was increased, and the same procedure was performed until one finds an averaged error estimate $[\bar{\eta}_2(\lambda_{p+1})]$, which is lower than its own value in the previous step $[\bar{\eta}_2(\lambda_p)]$. This means that a local minima λ^* of the function $\eta_2(\lambda)$ was found at an internal point of S_2 (this step could be seen in Fig. 2). Once λ^* is found, no more Lanczos bidiagonalization steps were required. This completes the first phase of the algorithm.

The second phase improves the accuracy of λ^* . This was achieved by adding the points around λ^* in set S_2 . The points were added by bisection in log-scale and the value of λ^* was being updated such that Eq. (11) is valid. This step was performed until the minimum distance between adjacent grid points around λ^* in S_2 reaches a user defined tolerance (10^{-4}). Thus, refined $\lambda = \lambda^*$ is the suitable regularization parameter.

Other popular techniques to determine regularization parameter are L-curve, generalized cross-validation (GCV) method, and LSQR method. Shaw et al.¹⁷ showed that LSQR was faster and quantitatively more accurate than L-curve and GCV methods. The LSQR method is based on the minimization of residual $\|b - Ax\|_2^2$. The detailed description of regularized LSQR method is omitted here, interested readers can refer to Algorithm 1 in Ref. 17, which minimizes the squared ℓ_2 norm of residual vector (r). The main aim of the present study is to show that the proposed method is computationally more efficient than other popular techniques, without compromising the reconstructed image quality.

It will also be shown in the next subsections that the proposed error estimate (η_2) is generic in nature and can be utilized (for example, instead of r in LSQR-based method proposed in Ref. 17) for other popular model-based reconstruction techniques, with examples of traditional Tikhonov regularization, recently proposed exponential filtering,²⁴ and ℓ_1 - or TV-norm based regularization.

3.2 Traditional Tikhonov Regularization

The Tikhonov-based ℓ_2 norm smoothness constraint is widely utilized for solving the reconstruction problem. As seen in Eq. (5), the Tikhonov regularization solution can be written as

$$(\mathbf{A}^T \mathbf{A} + \lambda \mathbf{I})x_\lambda = \mathbf{A}^T b. \quad (17)$$

The SVD of the system matrix, i.e., its reduction to diagonal form, can be represented as

$$\mathbf{A} = \mathbf{U} \mathbf{\Sigma} \mathbf{V}^T, \quad (18)$$

where \mathbf{U} and \mathbf{V} are left and right orthogonal matrices and $\mathbf{\Sigma}$ is a diagonal matrix containing singular (spectral) values on its diagonal. Using the SVD of \mathbf{A} [Eq. (18)], the solution to Eq. (17) for this case can be rewritten as²⁴

$$x_\lambda = (\mathbf{V} \mathbf{\Sigma}^T \mathbf{\Sigma} \mathbf{V}^T + \lambda \mathbf{I})^{-1} \mathbf{V} \mathbf{\Sigma}^T \mathbf{U}^T b, \quad (19)$$

$$x_\lambda = \mathbf{V} \mathbf{\Sigma}_F^\dagger \mathbf{U}^T b, \quad (20)$$

where the filtered singular values $\mathbf{\Sigma}_F^\dagger$ is given as

$$\mathbf{\Sigma}_F^\dagger = \text{diag} \left(\frac{\phi_i}{\sigma_i} \right), \quad (21)$$

where σ_i is i 'th singular value of \mathbf{A} , and ϕ_i are the filter factors defined as²⁴

$$\phi_i = \frac{\sigma_i^2}{\sigma_i^2 + \lambda}. \quad (22)$$

Rewriting Eq. (17) in terms of residual [Eq. (9)] makes

$$\mathbf{A}^T r_\lambda = \lambda x_\lambda, \quad (23)$$

where r_λ is the residue expressed in Eq. (9). x_λ can be evaluated using Eq. (20). Substituting $\mathbf{A}^T r_\lambda$ with λx_λ in Eq. (8), the expression becomes

$$\eta_2(\lambda) = \frac{\|r\|_2 \|x_\lambda\|_2}{\|\mathbf{A} x_\lambda\|_2}. \quad (24)$$

For the case of linear systems treated by Tikhonov method, above representation of the error estimate becomes numerically much more effective than Eq. (8). This estimate can be utilized in the framework of Algorithm 1 (especially in steps 8 to 14) to determine the required regularization parameter.

3.3 Exponential Filtering or Showalter's Method

The exponential filtering method was recently proposed for PA image reconstruction.²⁴ This method considers the exponential filtering of singular values of PA system matrix (\mathbf{A}). This

filtering was applied in the Tikhonov framework with solution being determined using Eq. (20) with a difference that the filter factors (ϕ_i 's) in this case are written as

$$\phi_i = 1 - \exp(-\sigma_i^2/\lambda). \quad (25)$$

Similar to Eq. (17), the solution can be uniquely determined by the consistent linear system:

$$(\mathbf{A}^T \mathbf{A} + \lambda \mathbf{R}^T \mathbf{R})x_\lambda = \mathbf{A}^T b, \quad (26)$$

which implies

$$\mathbf{A}^T r_\lambda = \lambda \mathbf{E} x_\lambda, \quad (27)$$

where $\mathbf{E} = \mathbf{R}^T \mathbf{R}$ is diagonal regularization matrix. Comparing Eqs. (20) and (26), the \mathbf{E} in this case can be constructed as

$$\mathbf{E} = \mathbf{R}^T \mathbf{R} = \frac{1}{\lambda} \mathbf{V} \mathbf{\Sigma}^T \mathbf{F} \mathbf{\Sigma} \mathbf{V}^T, \quad (28)$$

where \mathbf{F} is a diagonal filtering matrix, whose i 'th diagonal element can be constructed from filter factors defined as

$$\mathbf{F}_i = \frac{1}{\exp(\sigma_i^2/\lambda) - 1}. \quad (29)$$

Thus, i 'th diagonal element of \mathbf{E} can be written as

$$\mathbf{E}_i = \frac{\sigma_i^2/\lambda}{\exp(\sigma_i^2/\lambda) - 1}. \quad (30)$$

Substituting Eq. (27) in Eq. (8), the expression for error estimate becomes

$$\eta_2(\lambda) = \frac{\|r\|_2 \|\mathbf{E} x_\lambda\|_2}{\|\mathbf{A} \mathbf{E} x_\lambda\|_2}. \quad (31)$$

Now similar to the traditional Tikhonov method, one can use this expression in the framework of Algorithm 1 to determine the required regularization parameter (λ).

Local regularization parameter $\lambda^* = \lambda_p$ at which $\eta_2(\lambda_p)$ is minimum. Follow steps 8 to 14 of Algorithm 1 to find required λ .

3.4 ℓ_1 Norm or Total Variation-Norm Based Regularization Method

The ℓ_1 and total variation (TV) norms are sparsity promoting norms, which have been previously utilized in various image reconstruction applications.^{25,26} In this scheme, the cost function to be minimized becomes as

$$\arg \min_{x \in \mathbf{R}^{n^2}} \|\mathbf{A}x - b\|_2^2 + \lambda \|X\|_*, \quad (32)$$

where $\|\mathbf{X}\|_*$ is either ℓ_1 norm or TV term. \mathbf{X} is the matrix form of vectorized image x . For ℓ_1 -norm case:

$$\|\mathbf{X}\|_* = \|x\|_1. \quad (33)$$

The TV term is widely written as the ℓ_1 norm of gradient of image (x). Hence, for the TV-norm case:

$$\|X\|_* = \sum_{i=1}^{n^2} \|D_i x\|_1, \quad (34)$$

where D_i denotes the local finite difference operator (with boundary condition) at pixel i and $\sum_i \|D_i x\|_1$ is a discretization of the TV of x .²⁶ The solution x can be computed by minimizing Eq. (32).

The detailed description of these nonsmooth regularization schemes is beyond the scope of this study and these details can be found in Refs. 25–27. The exact algorithm that was utilized for finding the regularization parameter for ℓ_1 - or TV-norm regularization schemes was provided in Algorithm 2. Note that the initial step is similar to step 1 of Algorithm 1, i.e., the first step was to start with the i grid values chosen in interval $[\log(\lambda_{\min}), \log(\lambda_{\max})]$.

Then, the regularized solution (which minimized cost function) and the error estimate (η_2) was computed. For this step, the algorithm contained two loops. The outer loop started from a higher value of λ , and the inner loop solved Eq. (32). The outer loop progressively reduced the value of λ until the condition in step 7 of Algorithm 1 is met. The error estimate $\eta_2(\lambda)$ was evaluated using the following expression:

Algorithm 2 Algorithm for evaluation of regularization parameter for ℓ_1 - or TV-norm based regularization method.

1 Input: \mathbf{A} ; b ; $[\lambda_{\min}, \lambda_{\max}]$; \mathbf{X}_0 .

2 Output: local regularization parameter: λ^* .

1. while¹ $\eta_2(\lambda_p) < \eta_2(\lambda_{p+1})$ (i.e., step 7 of Algorithm 1)
2. while² $\frac{\Omega_k - \Omega_{k+1}}{\Omega_k + \Omega_{k+1}} \geq \text{Tol}$ (10^{-4}) (minimization of cost function Ω)

- Compute objective function for current iteration (k):

$$\Omega_k = \|\mathbf{A}x_k - b\|_2^2 + \lambda_p \|X_k\|_* \quad (35)$$

(X_k is the matrix form (dimension: $n \times n$) of vectorized image x_k (dimension: $n^2 \times 1$), with $\|\cdot\|_*$ being either ℓ_1 [Eq. (33)] or TV [Eq. (34)])

- i. $x_k = x_{k-1} + \mathbf{A}^T(b - \mathbf{A}x_{k-1})$
- ii. Form the matrix \mathbf{X}_k by reshaping x_k
- iii. SVD: $\mathbf{X}_k = \mathbf{U}\mathbf{S}\mathbf{V}^T$
- iv. Soft threshold of the singular values
 $\hat{\mathbf{S}} = \text{soft}(\text{diag}(\mathbf{S}), \lambda_p/2)$
- v. $\mathbf{X}_{k+1} = \mathbf{U}\hat{\mathbf{S}}\mathbf{V}^T$. Form x_{k+1} by vectorizing \mathbf{X}_{k+1}
- vi. Update $k = k + 1$

- Compute objective function for next iterate:

$$\Omega_{k+1} = \|\mathbf{A}x_{k+1} - b\|_2^2 + \lambda_p \|X_{k+1}\|_*$$

- End while²

3. $r_\lambda = b - \mathbf{A}x_{k+1}$. Compute $\eta_2(\lambda_p) = \frac{\|r_\lambda\|_2 \|\mathbf{A}^T r_\lambda\|_2}{\|\mathbf{A}\mathbf{A}^T r_\lambda\|_2}$

4. Update $p = p + 1$

5. End while¹

$$\eta_2(\lambda) = \frac{\|r_\lambda\|_2 \|\mathbf{A}^T r_\lambda\|_2}{\|\mathbf{A}\mathbf{A}^T r_\lambda\|_2}. \quad (36)$$

The suitable λ^* was selected as the one, which minimized $\eta_2(\lambda)$. Then, to accurately refine the value of λ , we iteratively added points to the grid around the minima λ^* , as described in steps 8 to 14 of Algorithm 1.

4 Numerical Experiments

Numerical experiments are ideal for comparing the quantitative accuracies and efficiency of the various methods as measuring actual initial pressure rise in experimental phantom is very challenging. In this work, three numerical phantoms were chosen to justify effectiveness of the proposed model. Since PA imaging is widely used for visualizing internal blood vessel structures, first is a numerical blood vessel network phantom with an initial pressure rise of 1 kPa. Another numerical phantom is a variation of the Derenzo phantom, which consists of small and large size circular targets distributions over the imaging region. Both these phantoms dimensions were 201×201 .

A bigger dimension, 301×301 , the blood vessel phantom was considered as a third phantom. In this case, 100 ultrasound detectors were utilized, thus making \mathbf{A} as big as $50,000 \times 90,601$. The size of vector b became $90,601 \times 1$. These phantoms are shown in Figs. 1(a), 1(e), and 1(i). The SNR of simulated data was kept at 40 dB to closely mimic the experimental data.

The main focus of this study was to compare the proposed LSQR method with Shaw et al.'s¹⁷ regularized LSQR method. This comparison was performed via running numerical simulations for the three phantoms introduced here. The study also showed that the proposed error estimate can be utilized with any regularization framework and to support the claim image reconstruction routines for Tikhonov regularization, exponential filtering, ℓ_1 -norm based regularization, and TV regularization frameworks were performed. A Linux workstation with dual eight-core Intel Xeon processors having a speed of 3.10 GHz with 128 GB RAM was used for all computations performed in this work.

5 Results and Discussion

The minimization of the error estimate (η_2) has been illustrated in Fig. 2. The circles show where $\eta_2(\lambda)$ was evaluated [Fig. 2(b)]. Adjacent circles were connected for visual clarity and the lines have no significance. The residue in the figure was minimized to find λ in Ref. 17. The local minima of residue curve [Fig. 2(a)] was situated close to the local minima of η_2 curve [Fig. 2(b)]. Once regularization is determined, the desired solution can be computed using Eq. (15).

For a 60 detectors' geometry PA system matrix [Figs. 1(a) and 1(e)], the required number of Lanczos bidiagonalization steps (k) turns out to be 44. This makes the size of matrix B_k^T as 45×44 (see Ref. 20), making computation of $(B^T B + \lambda I)^{-1}$, which has a dimension of 45×45 , inexpensive. The number of Lanczos bidiagonalization steps (k) required for the 100-detector case [Fig. 1(i)] was 77. The comparison of computation time between utilization of 201×201 dimension phantoms versus 301×301 dimension phantom is listed in Table 1.

The reconstruction results obtained for the blood vessel network using the regularized LSQR method¹⁷ and the proposed method are shown in Figs. 1(b) and 1(c). A one-dimensional cross-sectional plot for the reconstructed image along the red dotted line in the target image is shown in Fig. 1(d). This

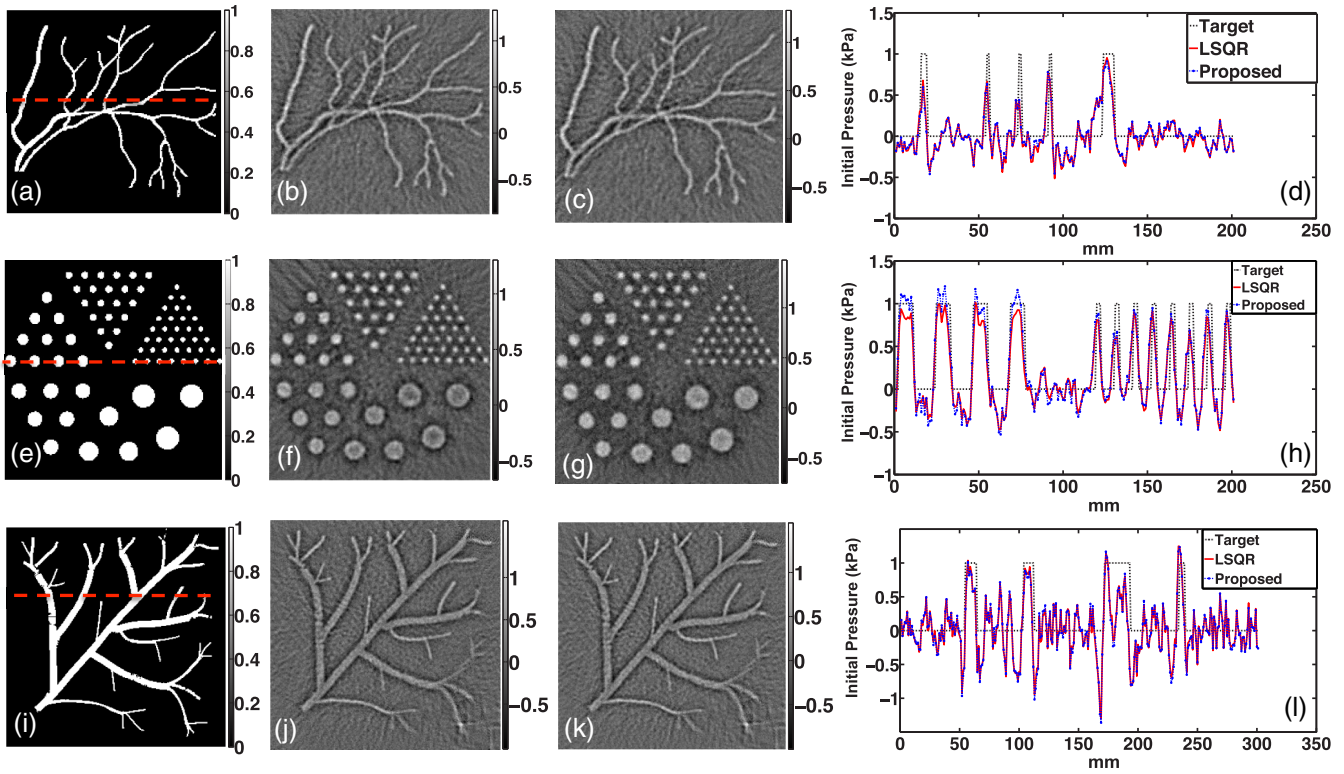


Fig. 1 The numerical phantoms used in this study. (a) Blood vessel network (dimension: 201×201), (e) Derenzo phantom (dimension: 201×201), and (i) blood vessel phantom (dimension: 301×301). Reconstructed images of these phantoms using (b,f,j) regularized LSQR method¹⁷ and (c,g,k) proposed method. (d,h,l) A 1-D cross-sectional plot for the reconstructed images along the dotted line in target phantoms. The corresponding computation time and quantitative metric are listed in Table 1.

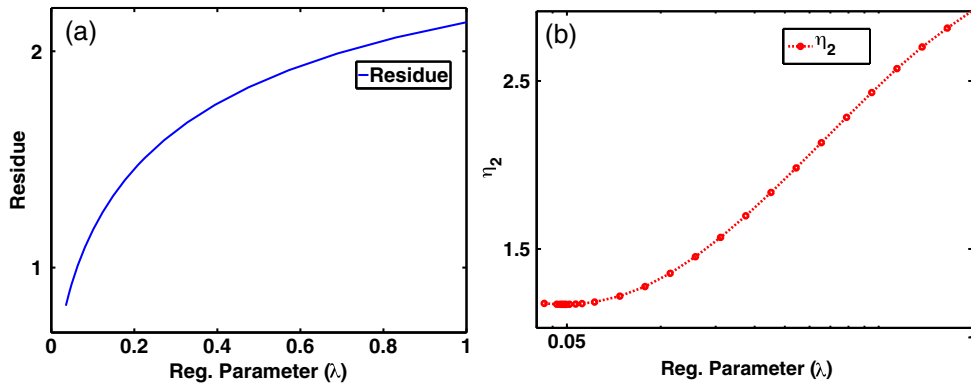


Fig. 2 The minimization of (a) residue ($\|b - Ax\|_2^2$) for $k = 44$ and (b) error estimate (η_2) [Eq. (8)] through Algorithm 1 for the phantom, as shown in Fig. 1(a).

Table 1 Performance comparison of two methods, regularized LSQR versus proposed methods for the results presented in Fig. 1.

Phantom	Regularized LSQR method ¹⁷			Proposed		
	Time (s)	λ	PC	Time (s)	λ	PC
Blood vessel network	~412	0.0423	0.59	~90	0.0594	0.58
Derenzo phantom	~424	0.0158	0.69	~96	0.0205	0.76
Blood vessel phantom	~1871	0.0890	0.534	~526	0.0672	0.529

Table 2 The computation time, regularization parameter, and PC for the results presented in Fig. 3.

Method	Computation	Blood vessel network		Derenzo phantom	
	Time (s)	λ	PC	λ	PC
Traditional Tikhonov regularization	~221	0.0035	0.58	0.0004	0.76
Exponential filtering ²⁴	~210	0.0077	0.57	0.0008	0.75
ℓ_1 -norm based regularization ²⁵	~617	0.0010	0.63	0.0010	0.59
TV-norm based regularization ²⁶	~581	0.0012	0.64	0.0011	0.65

plot shows that the performance of the proposed method in terms of quantitative accuracy of the reconstructed image is similar to the state-of-the-art regularized LSQR method. Figures 1(f)–1(h) show the similar results for the Derenzo phantom, which testify the ability to reconstruct the objects of different shapes and sizes. The results for the larger phantom (301 × 301 dimension, 100 detector points) are shown in Figs. 1(i)–1(l).

To check the performance of the image quality, a figure of merit, such as Pearson correlation (PC), was used for the comparison. PC is a quantitative metric that measures the degree of correlation between the target image and the reconstructed image. The PC is defined as¹⁸

$$PC(x, x^{\text{recon}}) = \frac{\text{COV}(x, x^{\text{recon}})}{\sigma(x)\sigma(x^{\text{recon}})}, \quad (37)$$

where x is the expected initial pressure distribution, x^{recon} is the reconstructed initial pressure distribution, COV denotes the covariance, and σ denotes the standard deviation. Higher value of PC corresponds to the accurate detectability of the target (i.e., spatial fidelity).^{18,28}

The proposed method is computationally much faster than previously proposed methods. Table 1 shows the comparison results, where it can be seen that there is little difference in PC, while the computation time is much lower for the proposed method (~4.5× speed up) compared to the regularized LSQR method proposed by Shaw et al.¹⁷ Note that the one-time system matrix building time (~181 s) was excluded from the computation time, as listed in Tables 1 and 2.

The proposed regularization method was also tested for other popular model-based reconstruction schemes, i.e., traditional Tikhonov regularization, exponential filtering of SVD-based²⁴ regularization, ℓ_1 -norm based regularization,²⁵ and TV-norm based regularization²⁶ technique to evaluate the regularization parameter and reconstruct the PA images. Figure 3 presents the reconstruction results for blood vessel network and Derenzo phantom obtained through these methods. Figures 3(a) and 3(b) show the reconstructed images obtained using Tikhonov regularization, and Figs. 3(c) and 3(d) show images obtained using recently proposed exponential filtering method.²⁴ The reconstruction results for nonsmooth regularization, such as ℓ_1 - and TV-norm based methods, are shown in Figs. 3(e)–3(f) and 3(g)–3(h), respectively. The ℓ_1 - and TV-norm based

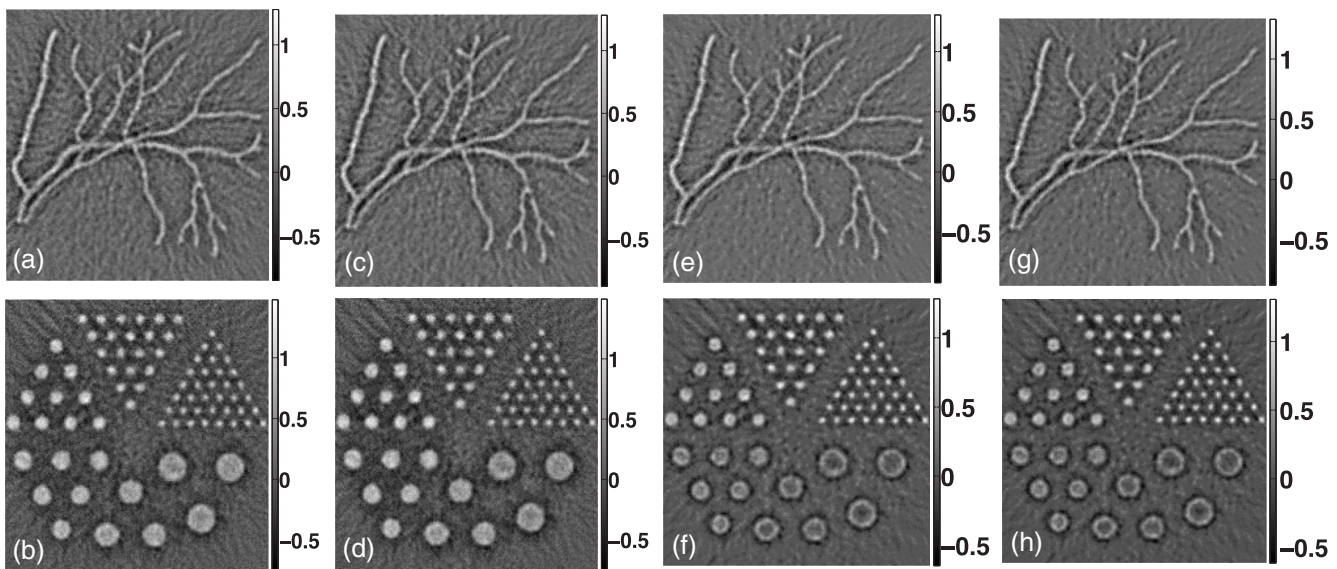


Fig. 3 Reconstructed images using (a and b) traditional Tikhonov regularization,²⁴ (c and d) exponential filtering of SVD-based reconstruction,²⁴ (e and f) ℓ_1 -norm based regularization,²⁵ and (g and h) TV-norm based regularization²⁶ for the two numerical phantoms [target phantoms are given in Figs. 1(a) and 1(e)], where the regularization parameter was determined using proposed error estimate minimization. The quantitative metrics are given in Table 2.

algorithm becomes expensive in computation for more iterations [Eq. (35)]. It is to be noted that the results presented for ℓ_1 - and TV-based reconstructions²⁵ are for 10 iterations, with ℓ_1 -norm based method being slightly more expensive in terms of computation (refer to Table 2). However, the reconstruction accuracy can be improved with a larger number of iterations. The algorithm to determine regularization parameter for nonsmooth regularization methods was described in Algorithm 2. As it can be seen, the proposed error estimate (η_2) is capable of determining the required regularization parameter both in the smooth and non-smooth regularization frameworks. The regularization parameter determined using the proposed η_2 estimate and the image quality metrics, PC, has been listed in Table 2.

The regularization schemes that are utilized in this work include smooth and nonsmooth regularizations. Among the smooth regularization (Tikhonov) schemes, we have implemented the proposed scheme both in dimensionality reduction frame work (regularized LSQR) as well as traditional Tikhonov frame work. From Tables 1 and 2, it is clear that the regularized LSQR method is computationally more efficient and observed reconstruction performance (in terms of PC) for both methods is same as expected. It should be noted that the Lanczos bidiagonalization was not utilized for nonsmooth regularization schemes, including the presented ℓ_1 - and TV-norm based ones. These (nonsmooth regularization schemes) were implemented in traditional fashion (same as traditional Tikhonov) as the main aim of this work was to show that the proposed error estimates have utility for any regularization frame work (traditional/reduced dimension combined with smooth/nonsmooth).

The assessment of image quality in emission tomography as well as biological imaging has been previously performed through figure of merits, such as PC.^{18,28} Even though the task-based image quality metrics²⁹ can better assess the reconstructed image quality, the use of residual errors (least-squares metric) in comparison of reconstruction algorithms performance (including the parameters used in them) has been a common practice across tomographic problems.³⁰ The estimate of these residual errors has been utilized in this work to find the appropriate reconstruction parameters; here, it is being regularization parameter. The future scope of this study is to validate the performance of proposed algorithm through experimental studies, which can further assure the efficiency and usability of proposed method.

6 Conclusions

The LSQR model has been extensively used and shown to be effective¹⁵ in full-view data cases ($m \gg n^2$), where there is no requirement of regularization. However, in limited data ($m \ll n^2$) cases, Tikhonov framework has to be used for regularizing the solution.¹⁷ Determining a suitable regularization parameter is important as the solution is sensitive to this choice. This study addressed the problem of determining the regularization parameter automatically based on error estimate (η_2) analysis without any prior information about the noise. Utilizing this with Lanczos bidiagonalization framework adds the advantage of reducing the dimensionality of the problem. This makes the proposed model highly computationally efficient and promising as compared to the other popular state-of-the-art techniques. The proposed method is generic in nature and can be used in any regularization framework to determine the regularization parameter. Here, it was also shown that the proposed

method is 4.5 times faster compared to existing state-of-the-art methods.

Acknowledgments

Authors would like to thank the anonymous reviewers for their thoughtful comments, which improved this work. This work was supported by Department of Biotechnology (DBT) Innovative Young Biotechnologist Award (IYBA) (Grant No.: BT/07/IYBA/2013-13), the Department of Biotechnology (DBT) Rapid Grant for Young investigator (RGYI) (Grant No.: BT/PR6494/GDB/27/415/2012), and DBT Bioengineering Grant (Grant No.: BT/PR7994/ MED/32/284/2013). The work of M.B. was supported by National Mathematics Initiative (NMI).

References

1. M. Xu and L. V. Wang, "Photoacoustic imaging in biomedicine," *Rev. Sci. Instrum.* **77**, 41101 (2006).
2. R. Li et al., "Assessing breast tumor margin by multispectral photoacoustic tomography," *Biomed. Opt. Express* **6**(4), 1273–1281 (2015).
3. G. Diot, A. Dima, and V. Ntziachristos, "Multispectral opto-acoustic tomography of exercised muscle oxygenation," *Opt. Lett.* **40**(7), 1496–1499 (2015).
4. B. Z. Chen et al., "Photoacoustic imaging of cerebral hypoperfusion during acupuncture," *Biomed. Opt. Express* **6**(9), 3225–3234 (2015).
5. X. Li et al., "High resolution functional photoacoustic tomography of breast cancer," *Med. Phys.* **42**(9), 5321–5328 (2015).
6. M. Pramanik et al., "Design and evaluation of a novel breast cancer detection system combining both thermoacoustic (TA) and photoacoustic (PA) tomography," *Med. Phys.* **35**(6), 2218–2223 (2008).
7. T. N. Erpelding et al., "Sentinel lymph nodes in the rat: noninvasive photoacoustic and US imaging with a clinical US system," *Radiology* **256**(1), 102–110 (2010).
8. M. Nasiriavanaki et al., "High-resolution photoacoustic tomography of resting-state functional connectivity in the mouse brain," *Proc. Natl. Acad. Sci. U. S. A.* **111**(1), 21–26 (2014).
9. P. van Es et al., "Initial results of finger imaging using photoacoustic computed tomography," *J. Biomed. Opt.* **19**(6), 060501 (2014).
10. L. A. Kunyansky, "Explicit inversion formulae for the spherical mean Radon transform," *Inverse Probl.* **23**(1), 373–383 (2007).
11. Y. Xu, D. Feng, and L. V. Wang, "Exact frequency-domain reconstruction for thermoacoustic tomography: I. Planar geometry," *IEEE Trans. Med. Imaging* **21**(7), 823–828 (2002).
12. Y. Xu and L. V. Wang, "Universal back-projection algorithm for photoacoustic computed tomography," *Phys. Rev. E* **71**, 16706 (2005).
13. G. Paltauf et al., "Iterative reconstruction algorithm for optoacoustic imaging," *J. Acoust. Soc. Am.* **112**(4), 1536–1544 (2002).
14. X. L. Dean-Ben et al., "Accurate model-based reconstruction algorithm for three-dimensional optoacoustic tomography," *IEEE Trans. Med. Imaging* **31**(10), 1922–1928 (2012).
15. A. Rosenthal, V. Ntziachristos, and D. Razansky, "Acoustic inversion in optoacoustic tomography: a review," *Curr. Med. Imaging Rev.* **9**(4), 318–336 (2013).
16. K. Wang et al., "Investigation of iterative image reconstruction in three-dimensional optoacoustic tomography," *Phys. Med. Biol.* **57**(17), 5399–5424 (2012).
17. C. B. Shaw et al., "Least squares QR-based decomposition provides an efficient way of computing optimal regularization parameter in photoacoustic tomography," *J. Biomed. Opt.* **18**(8), 080501 (2013).
18. J. Prakash et al., "Basis pursuit deconvolution for improving model-based reconstructed images in photoacoustic tomography," *Biomed. Opt. Express* **5**(5), 1363–1377 (2014).
19. B. E. Treeby and B. T. Cox, "k-Wave: MATLAB toolbox for the simulation and reconstruction of photoacoustic wave fields," *J. Biomed. Opt.* **15**(2), 021314 (2010).

20. P. C. Hansen, *Rank Deficient and Discrete ill-Posed Problems*, Society for Industrial and Applied Mathematics, Philadelphia (1998).
21. C. Brezinski, G. Rodriguez, and S. Seatzu, "Error estimates for the regularization of least squares problems," *Numer. Algorithms* **51**(1), 61–76 (2009).
22. L. Reichel, G. Rodriguez, and S. Seatzu, "Error estimates for large-scale ill-posed problems," *Numer. Algorithms* **51**(3), 341–361 (2009).
23. C. C. Paige and M. A. Saunders, "LSQR: an algorithm for sparse linear equations and sparse least squares," *ACM Trans. Math. Software* **8**(1), 43–71 (1982).
24. M. Bhatt, S. Gutta, and P. K. Yalavarthy, "Exponential filtering of singular values improves photoacoustic image reconstruction," *J. Opt. Soc. Am. A* **33** (9), 1785–1792 (2016).
25. A. Majumdar and R. K. Ward, "Nuclear norm-regularized SENSE reconstruction," *J. Magn. Reson. Imaging* **30**(2), 213–221 (2012).
26. Y. H. Xiao and J. F. Yang, "Alternating algorithms for total variation image reconstruction from random projections," *Inverse Probl. Imaging* **6**(3), 547–563 (2012).
27. A. Majumdar and R. K. Ward, "An algorithm for sparse MRI reconstruction by Schatten p-norm minimization," *Magn. Reson. Imaging* **29**(3), 408–417 (2011).
28. J. Kuntz et al., "Constrained reconstructions for 4-D intervention guidance," *Phys. Med. Biol.* **58**(10), 3283–3300 (2013).
29. A. Petschke and P. J. La Riviere, "Comparison of photoacoustic image reconstruction algorithms using the channelized hotelling observer," *J. Biomed. Opt.* **18**(2) 026009 (2013).
30. W. S. Phillips and M. C. Fehler, "Traveltime tomography: a comparison of popular methods," *Geophysics* **56**(10), 1639–1649 (1991).

Manish Bhatt received his BTech degree from the National Institute of Technology, Hamirpur, Himachal Pradesh, India, in 2011. Currently, he is a graduate student at the National Mathematics Initiative, Indian Institute of Science (IISc), Bangalore, India.

Atithi Acharya is currently an undergraduate student in the Department of Physics, Indian Institute of Science (IISc), Bangalore, India. His research interests include medical physics, biomedical optics, and scientific computing.

Phaneendra K. Yalavarthy received his MSc degree in engineering from the Indian Institute of Science, Bangalore, India, and his PhD degree in biomedical computation from Dartmouth College, Hanover, New Hampshire, in 2007. He is an associate professor in the Department of Computational and Data Sciences, Indian Institute of Science, Bangalore. His research interests include medical image computing, medical image analysis, and biomedical optics.